Computers and Fluids 162 (2018) 26–38

Contents lists available at ScienceDirect

Computers and Fluids

journal homepage: www.elsevier.com/locate/compfluid

Numerical simulation of turbulent spots generated by unstable wave packets in a hypersonic boundary layer

Pavel V. Chuvakhov[a,b,*], Alexander V. Fedorov[b,a], Anton O. Obraz[a,b]

[a] Central Aerohydrodynamic Institute (TsAGI), 1 Zhukovskogo Str., Zhukovsky, Moscow Region, 140180, Russian Federation
[b] Moscow Institute of Physics and Technology (MIPT), 9 Institutskiy per., Dolgoprudny, Moscow Region, 141701, Russian Federation

ARTICLE INFO

Article history:
Received 1 August 2017
Revised 23 November 2017
Accepted 3 December 2017
Available online 5 December 2017

Keywords:
Computational fluid dynamics
Numerical simulation
Turbulent spot
Wave packet
Boundary layer
Stability

ABSTRACT

The generation of a turbulent spot by an unstable wave packet propagating in a Mach-6 flat-plate boundary layer is considered. The asymptotic shape of the wave packet is obtained in the far field from the excitation point using linear stability theory. Unsteady boundary conditions are formulated for direct numerical simulation. They allow for excitation of a well-developed wave packet with specified amplitude, skipping the linear growth stage. Robustness of these boundary conditions for modeling of the nonlinear breakdown of unstable wave packets into turbulent spots is examined.

1. Introduction

Turbulization of the boundary layer flow on a hypersonic vehicle (HV) leads to significant increase of viscous drag and heat flux to the surface. Therefore, laminar-turbulent transition (LTT) is a key problem for design of modern super- and hypersonic flight vehicles. There are various scenarios of LTT depending on free-stream parameters and external disturbance spectra [1]. Free flight of HV usually suggests small level of external disturbance and smooth walls of relatively low wall-to-edge temperature ratios. Under these conditions, the LTT process involves the three stages: (1) receptivity of the boundary-layer flow to external disturbances, (2) exponential growth of instabilities (normal modes) in the boundary layer, (3) nonlinear breakdown to turbulence. The wall cooling is known to stabilize the first mode (predominantly oblique waves related to Tollmien–Schlichting waves at low speeds) and destabilize the second mode (predominately plane waves with their fronts being normal to the free stream).

A state-of-the-art method for engineering applications to predict the transition onset is the e^N method [2,3]. It is assumed that the boundary layer disturbances are equally excited all over the body surface and have a wide spectrum. Physical situations, where this assumption is valid, could be transition induced by solid particulates, distributed roughness and kinetic fluctuations [4].

In many cases the nonlinear breakdown goes through birth, growth and merging of initially localized patches of turbulent flow, also referred to as turbulent spots. The flow has an intermittent behavior [5]. An intermittency factor γ is introduced as a portion of time when the flow is turbulent at a given point. Numerous experimental investigations (see reviews [6–8]) showed that a typical turbulent spot has roughly a triangular shape, and its propagation is described by the three parameters: leading and trailing edge velocities U_{le}, U_{te} and spreading half-angle $\beta_{1/2}$ (Fig. 1).

Assuming that turbulent spots are originated in a narrow region near the transition onset point $x = x_t$, Narasimha [9] derived a simple approximation of intermittency distribution for a two-dimensional flat plate flow:

$$\gamma(x) = 1 - \exp\left(-\frac{n\sigma}{U_\infty}(x - x_t)^2\right), \ x > x_t.$$

Here n is the spot birth rate per unit length, σ is the shape (or propagation) factor which is calculated as [10]:

$$\sigma = \tan(\beta_{1/2}) \cdot \left(\frac{U_\infty}{U_{te}} - \frac{U_\infty}{U_{le}}\right).$$

Similar relationships were derived for conical mean flows [11].

Fischer [6] summarized experimental data and showed that $\beta_{1/2}$ decreases with Mach number. Experiments [12] in quiet wind

Abbreviations: LTT, Laminar-turbulent transition; LST, Linear stability theory; DNS, Direct numerical simulation; LN, HN, Cases of lower and higher values of N-factor.

* Corresponding author at: Central Aerohydrodynamic Institute (TsAGI), 1 Zhukovskogo Str., Zhukovsky, Moscow Region, 140180, Russian Federation.

E-mail addresses: pavel.chuvakhov@tsagi.ru, pavel.chuvakhov@phystech.edu (P.V. Chuvakhov), fedorov@falt.ru (A.V. Fedorov), obraz89@gmail.com (A.O. Obraz).

https://doi.org/10.1016/j.compfluid.2017.12.001
0045-7930/

Nomenclature

$(x,\ y,\ z)$	Streamwise, wall-normal and spanwise Cartesian coordinates
$(u,\ v,\ w)$	Velocity components
σ	Shape (or propagation) factor of a turbulent spot
T_r	Recovery temperature
M	Mach number
Re	Reynolds number
$\alpha,\ \beta,\ \omega$	Streamwise and spanwise wavenumbers, circular frequency of disturbance
c	Phase speed of disturbance
x_0	Neutral point
S	Eikonal, $S=\int_{x_0}^{x}\alpha(\omega,\beta,\tilde{x})d\tilde{x}$
N	N-factor, $N=-S_i$
$\hat{\boldsymbol{A}}_s$	Normalized vector of disturbance eigenfunction
x_{in}	x-coordinate of the input boundary (beginning of a truncated computational subdomain)
ε	Maximum of the wall pressure disturbance envelope, $p'_w(t,z,x_{in})$, (wave packet hump)
$\Re[f],\ \Im[f]$	Real and imaginary parts of complex quantity: $f=\Re[f]+i\cdot\Im[f]$

Superscript

$*$	Dimensional value
$'$	Fluctuation (disturbance)

Subscript

e	Boundary layer edge
∞	Free stream
0	Isentropic stagnation value
w	Wall
s	Saddle point
$r,\ i$	Real and imaginary parts of a complex quantity

tunnels ($M_e\approx 6,\ T_w/T_0\approx 0.69$) partially confirm the results [6]. However, the value of $\beta_{1/2}$ is defined ambiguously in [12]. It is overpredicted for all considered definitions of the turbulent spot edges. Significant scattering of $\beta_{1/2}$ from 2° to 14° was observed in high-enthalpy tunnels [13,14] ($M_e=5,\ T_w\approx 0.17T_e$).

Numerical simulations [15–21] show that the wall-to-stagnation (recovery) temperature ratio T_w/T_0 (T_w/T_r) has a dramatic impact on a turbulent spot shape. The spot has a distinct triangular form at the adiabatic wall condition, $T_w=T_r$. For the cold wall condition, $T_w=T_e$, the spot is elongated in x-direction: $\beta_{1/2}$ and U_{te} decrease, while U_{le} remains almost constant. Herein, the lateral spreading angles may differ significantly from Fischer's data [6]. Estimations of the shape factors σ from available numerical and experimental data are summarized in Fig. 2, with the assumption that $U_{le}=1,0$ and $U_{te}=0,5$ for Fischer's data. The low supersonic data ($M_e<3$) [17,22] are well correlated except one point predicted numerically. However, it is obvious that available data are insufficient to approximate σ for hypersonic boundary layers.

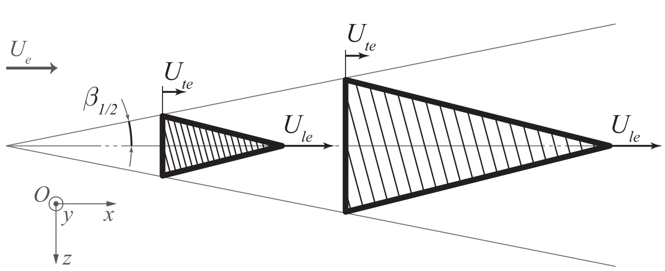

Fig. 1. Schematic view of turbulent spot propagation.

Table 1
Free-stream parameters.

M_∞	Re	T_∞	T_w/T_∞	T_w/T_0	Pr
6	10^6	300 K	1	≈ 0.12	0.72

Computations [15–18] assumed that the development of a turbulent spot does not depend on the history of its formation. The spots are excited almost instantaneously by a vortical source localized in the boundary layer. However, a natural turbulent spot forms differently. It is resulted from the wave packet, which, in turn, forms at the linear stage of instability growth and amplifies to a certain critical level. To our knowledge, this was taken into consideration in one series of experiments [12,23,24] as well as in the numerical simulations [19–21,25–27], where a wall-localized blow–suction boundary condition was used to generate unstable wave packets. To capture linear, nonlinear and turbulent stages of the wave-packet development, the computations were performed in long computational domains with grids having about 5×10^8 nodes (e.g. [25]). Nevertheless, such domains and grids are still insufficient to obtain a well-developed turbulent spot and investigate its dynamics.

In this paper, it is suggested to simulate the linear stage of unstable wave packets with the help of the linear stability theory (LST) and the e^N method. Using eigenfunctions of the dominant instability predicted by LST, the unsteady boundary conditions are derived in order to induce a wave packet in a given station. This condition is used as an inflow boundary condition for direct numerical simulations (DNS) of the nonlinear stage of LTT. Since the linear stage is omitted and corresponding lengthy part of computational domain is no longer present in DNS, the computational cost is reduced dramatically. The approach is applied to the development of second-mode wave packets in the boundary-layer flow on a flat plate at the free-stream Mach number $M_\infty=6$.

2. LST wave packets

Consider a supersonic flow of a compressible viscous gas past a flat plate with a sharp leading edge. The axes $(x,\ y,\ z)$ are directed streamwise, normal to the wall and spanwise, respectively (illustrated in Fig. 1); the line $(x,y)=(0,0)$ coincides with the plate leading edge. The Navier–Stokes equations are considered in the non-dimensional form: $(x,y,z)=(x^*,y^*,z^*)/L^*$, $t=t^*U^*_\infty/L^*$, $(u,v,w)=(u^*,v^*,w^*)/U^*_\infty$, $p=p^*/(\rho^*U^{*2}_\infty)$, $T=T^*/T^*_\infty$, where L^* is a characteristic length scale. Reynolds number $Re=U^*_\infty\rho^*_\infty L^*/\mu^*_\infty$ is assumed high enough to neglect the effects associated with viscous-inviscid interaction; i.e. the bow shock wave is weak and the free-stream parameters (see Table 1) are approximately equal to those at the upper boundary-layer edge. The Sutherland's law is used to approximate the dynamic viscosity coefficient:

$$\mu^*=\mu^*_\infty\frac{T^*_\infty-S^*}{T^*-S^*}\left(\frac{T^*}{T^*_\infty}\right)^{3/2},$$

where $S^*=110.4\ K$. For LST analysis, the mean-flow profiles $U(\eta), T(\eta)$, $\eta=y(Re/x)^{1/2}$ are obtained using a self-similar solution of zero-gradient compressible boundary layer equations (compressible Blasius solution). The Navier–Stokes solution shows that the upper-edge flow parameters are very close to the corresponding free-stream parameters: $\frac{Re_e(x)-Re_\infty}{Re_\infty}<0.0076$, $\frac{T^*_e(x)-T^*_\infty}{T^*_\infty}<0.0085$ and $-\frac{U^*_e(x)-U^*_\infty}{U^*_\infty}<0.0006$ at $x>1$. This leads to the excellent agreement of the mean-flow profiles (solid lines in Fig. 3) with the corresponding profiles of Navier–Stokes solution (symbols).